

CHAPTER 1

INTRODUCTION

1.1 PROJECT BACKGROUND

The study on the behaviour of viscoelastic fluid flow is important because of the various engineering application mainly on the polymer processing such as injection moulding and film blowing. In these applications, viscoelastic fluid flows through a series of pipe with different cross sectional areas and contraction ratios.

Viscoelastic material such as polymer and blood exhibit both viscous and elastic property when stress is applied. When viscoelastic fluid flows through a three – dimensional gradual planar contraction, an extreme near-wall velocity overshoots termed as the cat's ear is observed. The cat's ear profile is proven to be produced solely because of the smooth contraction and dependant highly on the elastic property of the liquid (Poole *et al.* (2009)).

The study of the cat's ear profile has been conducted previously by many researches. However, the effect of temperature on this phenomenon is not available in the literature. This project will be focusing on numerical simulations using computational fluid dynamics software to study the effect of wall temperature on the presence of the cat's ear discussed in the next section.

1.2 PROBLEM STATEMENT

Experimental and numerical investigations on isothermal viscoelastic flows through a gradual contraction have revealed an interesting flow phenomenon where large velocity overshoots near the sidewalls are observed. This phenomenon is called cat's ear due to its appearance. These cat's ears, which is an inherent feature of a viscoelastic fluid, have been found to be highly dependent on the elastic property of the fluid. The temperature effect on this cat's ear phenomenon however is not available in the literature.

1.3 OBJECTIVE

The main objective for this study is to conduct CFD simulations using a commercial CFD code of a viscoelastic fluid flowing through a three dimensional section and study the temperature effects on the cat's ear phenomenon.

1.4 SCOPE OF STUDY

A CFD simulation will be performed on viscoelastic fluids, 0.3% w/w and 0.005% w/w polyacrylamide (PAA) in an 8:1 planar gradual contraction section in two different operating conditions. The first condition exhibit standard operating condition with temperature of the wall is the same as the temperature of the fluid $T_{wall} = T_{fluid}$. The second condition will incorporate the effects of the wall temperature $T_{wall} \neq T_{fluid}$ on the presence of the cat's ear. For the second condition, PAA solution with concentration of 50ppm or 0.005% w/w is used. The use of different solution for the temperature effect study is due to the availability of rheological correlation for the solution with temperature based on the literature by Mu-Hoe Yang (2000).

In order to simulate the cat's ear phenomenon, a computational fluid dynamics (CFD) software, Fluent v6.1.22, will be utilized to perform the numerical simulation of the viscoelastic fluid flow. Prior to the simulation, Gambit v2.1.6 will be used to build the geometric modelling and meshing of the three dimensional 8:1 planar gradual contraction.

CHAPTER 2

LITERATURE REVIEW

2.1 VISCOELASTICITY

Viscoelastic fluid shows both viscous and elastic characteristics when undergoing deformation or when experiencing stress (Meyers and Chawla (1999)). Viscous alone is the resistance to flow. Viscosity is the ratio of the shearing stress to the velocity gradient in a fluid. Elastic is the property of a material to strain instantaneously when stretched and will return to the original configuration when stress is removed.

All viscoelastic fluid is non-Newtonian. Viscoelasticity is the behaviour between the two extremes Newtonian behaviour and the Hookean elastic response. Increase in strain at constant stress (creep) and decrease in stress at constant strain (relaxation) are both viscoelastic effects (Brinson and Brinson (2008)). Compared to purely elastic material, a viscoelastic substance loses some energy (in terms of viscous dissipation and disposed of as heat) when a load is applied, then removed. Hysteresis is observed in the stress-strain curve with the area of the loop being equal to the energy lost during the loading cycle (Meyers and Chawla (1999)). The red area (shown in the Figure 1 below) is a hysteresis loop and shows the amount of energy lost (as heat) in a loading and unloading cycle.

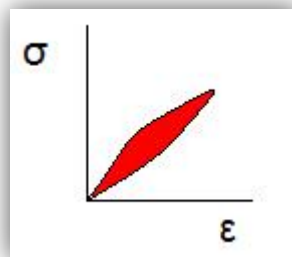


Figure 1: Stress-strain curves for a viscoelastic material

2.2 POLYACRYLAMIDE

Polyacrylamide is a viscoelastic shear thinning fluid and generally thought of as having a 'very flexible' molecular structure (Walters *et al.* (1990)). The fluid has more pronounced elastic properties than other water-soluble polymers such as xanthan gum or carboxymethylcellulose. The polyacrylamide used during the investigation was Separan AP 273 E with a molecular weight of approximately 2×10^6 g/mol. The rheological data for the polymer solution is obtained from Keegan (2009).

The International Union of Pure and Applied Chemistry (IUPAC) name for polyacrylamide is poly(2-propenamide) or poly(1-carbamoylethylene) is a polymer formed from acrylamide monomers that can also be readily cross-linked. Polyacrylamide is a non-toxic compound, but unpolymerized acrylamide which is neurotoxin can be present (Deryck (2007)). Thus, it needs to be handled using safe laboratory practice.

It is highly water-absorbent in the cross-linked form. It forms a soft gel used in several applications such as polyacrylamide gel electrophoresis (a method to quantify protein in solutions containing phosphoprotein) and in manufacturing soft contact lenses. In the straight-chain form, it is also used as a thickener and suspending agent. More recently, it has been used as sub dermal filler for aesthetic facial surgery.

The polymer is also widely used in several engineering application. In waste water management and paper making, polyacrylamide is used to flocculate or coagulate solids in a liquid (Keegan (2009)). Other than that, it is also used in subsurface applications such as oil production. High viscosity aqueous solutions can be obtained with low concentrations of polyacrylamide polymers, and these can be injected into the reservoir to control water production from the well (R.F. Legere (1977)).

The rheological behavior of polyacrylamide (PAA) solution (Mu-Hoe Yang (2000)) discusses the effects of concentration and temperature on the power law parameters, k and n . It was found that the yield stress, τ of the PAA solution decreased with increasing temperature and increased with increasing concentration. Moreover, the consistency coefficient, k of PAA solution increased meanwhile the flow behavior index, n of PAA solution decreased with increasing temperature. As the concentration increases, the value of k increases meanwhile the value of n decreases.

It was also found that the effect of temperature on the τ , k and n of PAA solution of different concentrations followed an Arrhenius-type relationship. The following Arrhenius relations express the relationship between the temperature and rheological characteristics (Mu-Hoe Yang (2000)).

$$\tau = \tau_o \exp\left(\frac{Ea}{RT}\right) , \ln(\tau) = \ln(\tau_o) + \frac{Ea}{RT} \dots\dots\dots(1)$$

$$n = n_o \exp\left(\frac{Ea}{RT}\right) , \ln(n) = \ln(n_o) + \frac{Ea}{RT} \dots\dots\dots(2)$$

$$K = K_o \exp\left(\frac{Ea}{RT}\right) , \ln(K) = \ln(K_o) + \frac{Ea}{RT} \dots\dots\dots(3)$$

Where: τ_o , n_o and K_o represent constants,

Ea represents the activation energy, J/g-mol,

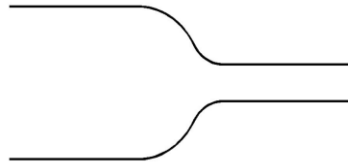
R represents the gas constant, J/g-mol K, and

T is the absolute temperature, K.

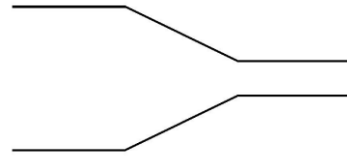
2.3 GEOMETRY

There is several type of contraction shown in the figure below.

(a) curved gradual contraction



(b) tapered gradual contraction



(c) abrupt contraction.

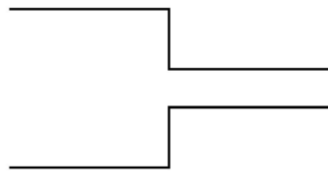


Figure 2: Examples of different types of contraction

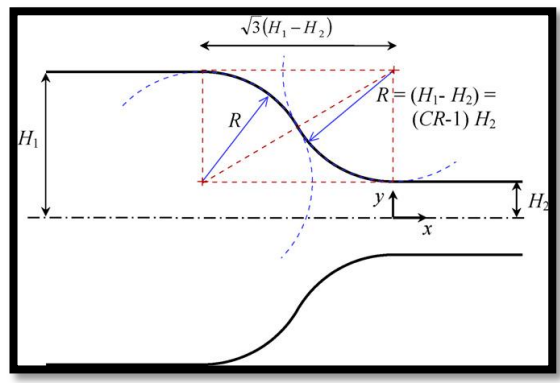


Figure3: Schematic of gradual contraction geometry. The depth of the geometry in the z direction is constant ($2H_1$)

In this project the above gradual contraction geometries based on R.J Poole *et al.* (2009) is used. A two dimensional projection of the geometry is used in the numerical simulation. It consists of two ducts connected by two arcs (one convex, the other is concave) of constant radius curvature $R = H_1 - H_2$. The larger duct which is the inlet having a square cross section and half height H_1 . The other one is the entrant having same width but different height $2H_2$. The contraction ratio is defined as $CR = H_1 - H_2$. The radius of the curvature can also be expressed as $R = (CR - 1)H_2$.

2.4 PROJECT OVERVIEW

Earlier research has been conducted related to the viscoelastic fluid flow through gradual contraction. Referring to velocity overshoots in gradual contraction flows by (R.J Poole et al. 2009), a numerical investigation is performed using the upper-convected Maxwell (UCM) and Phan-Thien-Tanner (PTT) models to study viscoelastic fluid flow through three-dimensional gradual planar contraction. The main purpose of the study is to investigate extreme near-wall velocity overshoots in similar geometries.

The study suggested that the cat's ear is a sole consequence of the smooth contraction. The velocity overshoots are purely elastic effects even without the inertial force. The value of Deborah number and contraction ratio plays an important role in the phenomenon. Other than that, increasing the inertial effects by increasing the Reynolds number will leads to more intense cat's ear i.e. inertia effects enhance the cat's ear phenomenon. The viscoelastic simulation using the UCM model shows that the cat's ear phenomenon can be reproduced using the UCM model under creeping flow condition. Creeping flow is a flow where the effective Reynolds number is very small i.e. less than one ($\ll 1$) such that the inertia effects can be ignored in comparison to the viscous resistance.

Experimental investigation into non-Newtonian fluid flow through gradual contraction geometries (Keegan (2009)) was conducted on polyacrylamide (PAA) and xantham gum (XG). Xantham gum is known to have lower elastic property in comparison to polyacrylamide. Cat's ear phenomenon was observed on both fluids. This is an indication that cat's ear phenomenon does not depends solely on the elasticity of the material.

CHAPTER 3

METHODOLOGY

3.1 PROCESS FLOW

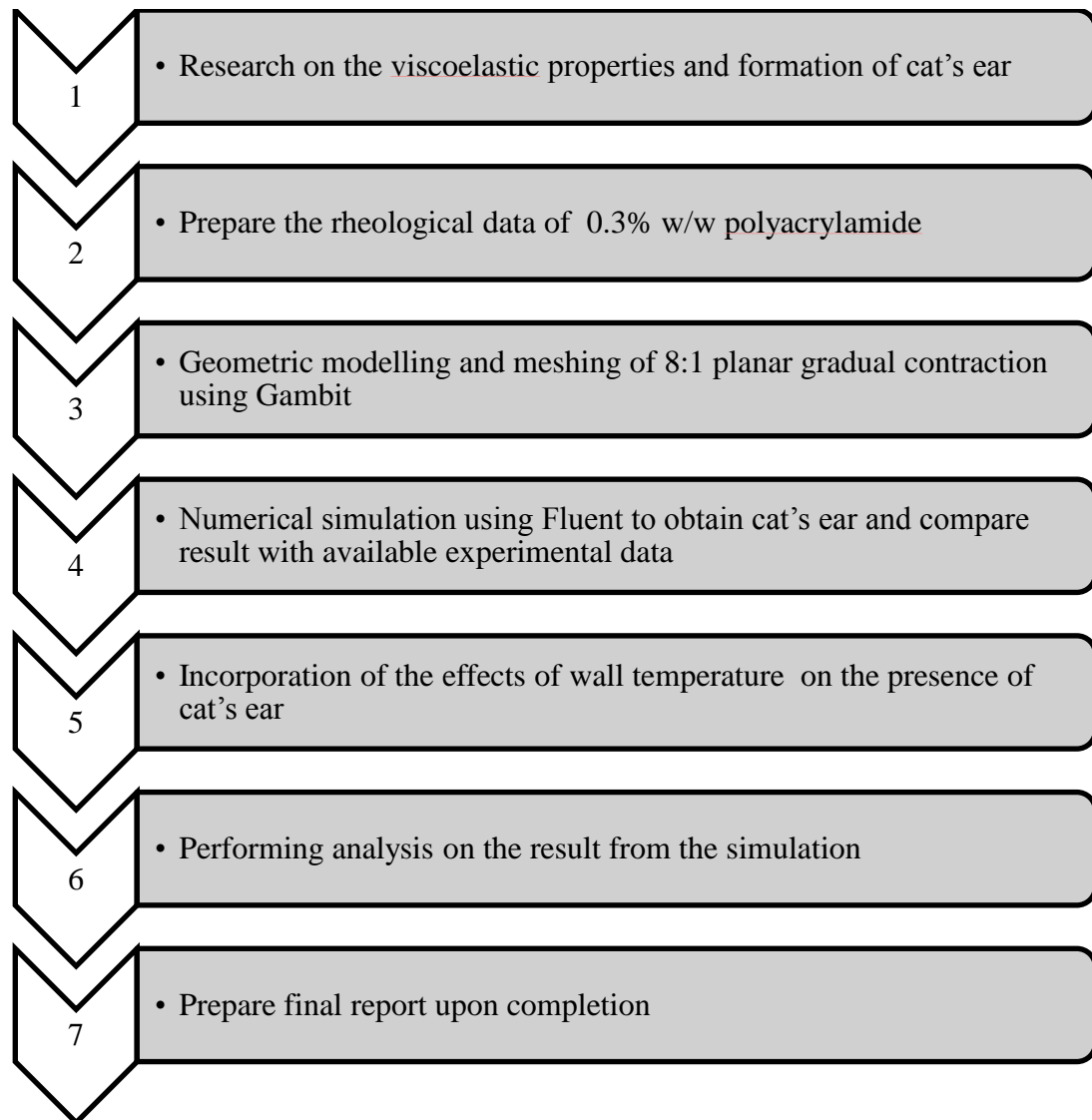


Figure 4: Project's Flow Chart

The first half (Final Year Project 1) of the project will cover up from step 1 until step 4. The rest will be covered during the Final Year Project 2.

3.2 GANTT CHART



No	Activities	Week														
		1	2	3	4	5	6	7	8	9	10	11	12	13	14	15
1	Selection of project topic	■	■													
2	Preliminary research work		■	■	■	■										
3	Submission of Preliminary Report					★										
4	Preparation of rheological data of polymer					■										
5	Geometric modelling and meshing					■	■	■								
6	Submission of Progress Report									★						
7	Seminar									★						
8	Numerical simulation to obtain cat's ear									■	■	■	■	■	■	■
9	Submission of Interim Report Final Draft															★
10	Oral Presentation															★

Table 1: Gantt chart for FYP I

No	Activities	Week														
		1	2	3	4	5	6	7	8	9	10	11	12	13	14	
1	Numerical simulation to obtain cat's ear	■	■	■												
2	Submission of Progress Report 1				★											
3	Incorporate Temperature Difference				■	■	■									
4	Submission of Progress Report 2									★						
5	Seminar (compulsory)									★						
6	Project work continues									■	■	■	■	■	■	■
7	Poster Exhibition												★			
8	Submission of Dissertation Final Draft															★
9	Oral Presentation															
10	Submission of Dissertation (hard bound)															

Table 2: Gantt chart for FYP II

Legends

-  Important Dateline
-  Process

CHAPTER 4

RESULT AND DISCUSSION

4.1 GEOMETRY PLOTTING IN GAMBIT

This section will explain on the geometry plotting, meshing, and boundary condition setting of a 3D 8:1 planar gradual contraction in Gambit.

4.1.1 8:1GRADUAL CONTRACTION PLOTTING

Contraction dimension: contraction ratio 8:1 based on (Poole *et al.* (2009)). All measurements are in millimetre (mm).

Contraction length, L	60.62
Length before contraction, L_i	2400
Length after contraction, L_o	1200
Width, w	80
Inlet height, D	80
Outlet height, d	10
Concave radius, R_1	35
Convex radius, R_2	35

Table 3: Dimension of the 8:1 gradual contraction

Figure 4 shows the schematic of 8:1 smooth gradual planar contraction. The height of the contraction varies gradually between the inlet duct height, $D=80\text{mm}$ and the outlet duct height $d=10\text{mm}$. The inlet and outlet are rectangular channels. The following term will be used in this project in reference to the contractions. Transverse and top to bottom profiles are measured on XY planes. The top and bottom of the contraction are the curved walls. Span wise and side to side profiles are those measured on XZ planes and the side walls are the plane walls.

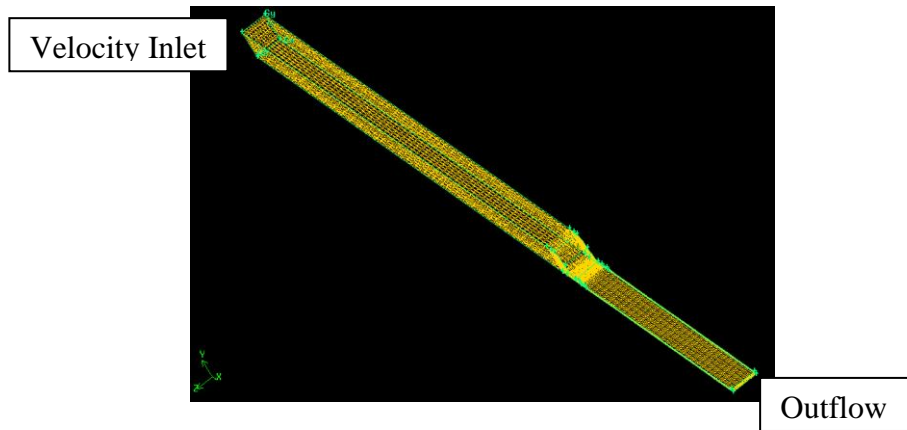


Figure 5: 3-D schematic of the 8:1 gradual contraction

4.1.2 8:1 GRADUAL CONTRACTION MESHING

The gradual contraction is constructed and meshed in Gambit v2. Figure below shows the meshing from different viewpoint. For simplicity purposes, only a quarter of the gradual contraction is plotted. The meshes used are structured and non-orthogonal, and were created in such a way that the cells are approximately aligned with the streamlines in the two-dimensional Newtonian case.

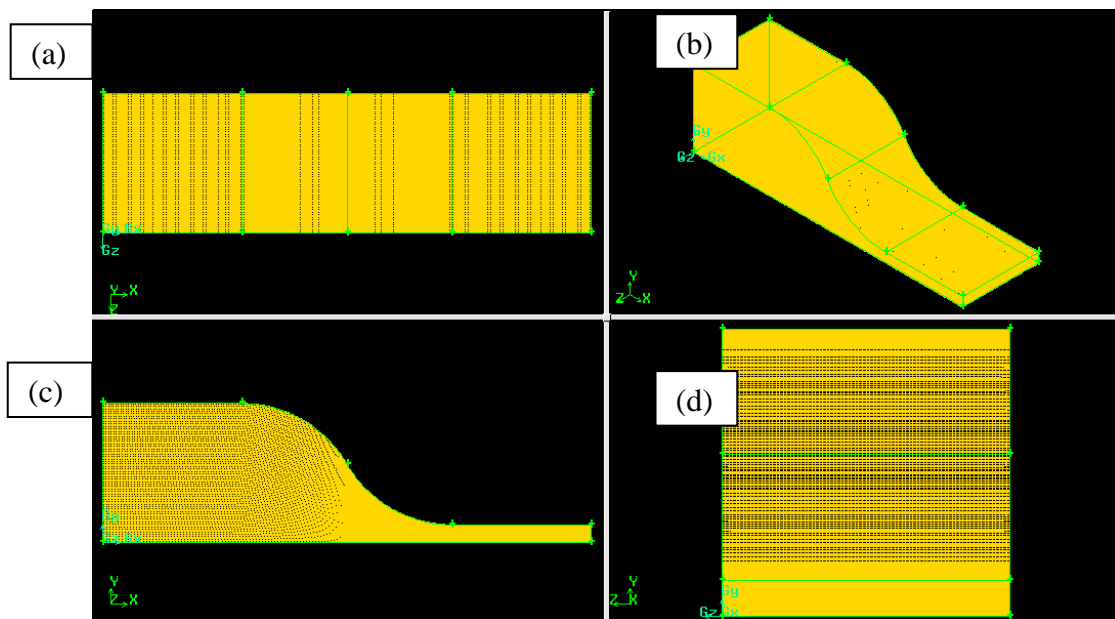


Figure 6: 8:1 gradual contraction meshing in gambit (a) top view in y-direction, (b) 3-D isometric view, (c) side view in z-direction and (d) front view in x- direction. Only part of the whole length is shown in detail.

4.1.3 BOUNDARY CONDITION

The boundary for the geometry is shown according to the colour code:

Blue : Velocity Inlet

Red : Outflow

White : Wall

Yellow: Symmetry

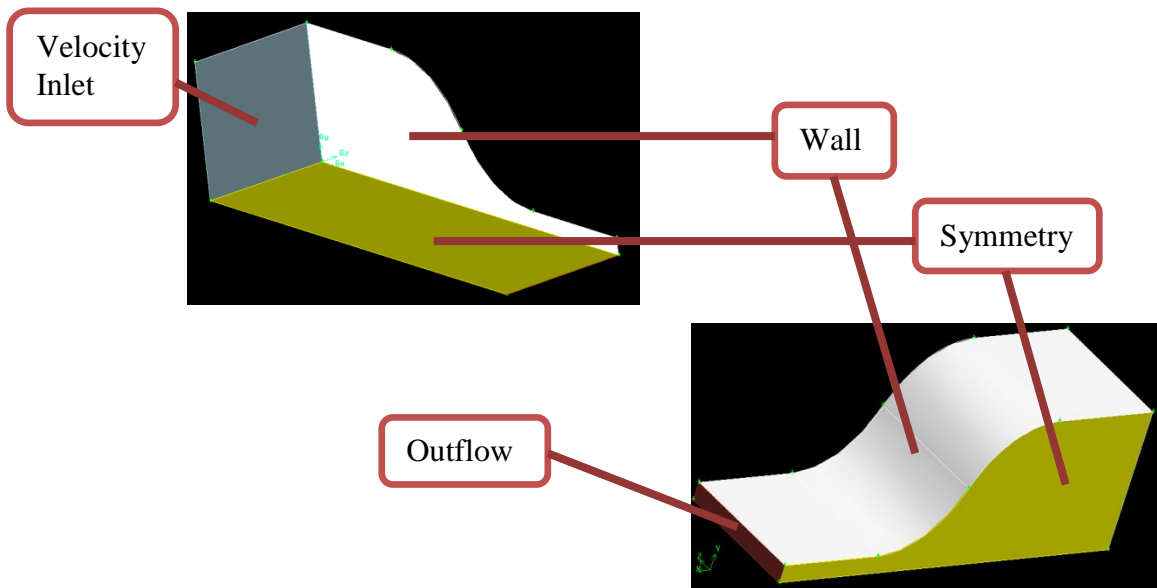


Figure 7: Boundary condition for planar gradual contraction segment

4.2 SIMULATION IN FLUENT

This section will explain the assumptions made, defined parameters, estimation of values, and graphical result of the simulation.

4.2.1 ASSUMPTION

The simulation is conducted based on the assumption that the flow is viscous and laminar in nature. Low Reynolds number is used to discard the effect of inertia on the cat's ear phenomenon i.e. under Stokes flow condition. Stokes flow is flow at very low Reynolds numbers, such that inertial forces can be neglected compared to viscous forces. Poole *et al.* (2009) demonstrated that inertia enhances the intensity of the cat's ear only to a certain extent and is not crucial in demonstrating the phenomenon.

Secondly, the fluid is considered continuous. That is, fluid properties such as density, pressure, temperature, and velocity are taken to be well-defined at infinitely small points, and are assumed to vary continuously from one point to another.

Thirdly, 0.3% polyacrylamide solution is modelled as incompressible fluid which means that the change in pressure does not affect the property of the fluid, i.e. the density is assumed constant throughout the flow, and hence, the incompressible Navier-Stokes equations are utilized.

Moreover, the flow is unidirectional from the inlet to the outlet of the gradual contraction. The walls of the contraction are assumed to be adiabatic indicating no heat loss to the surrounding. The walls are also stationary.

4.2.2 PARAMETER

Simulation in Fluent was conducted with the fluid described using a non-newtonian-power-law model. A Carreau-Yasuda model would give a better and comprehensive representative of the rheological behaviour of polyacrylamide solutions, but the model is not available in Fluent v6.1.22. Hence, power law model,

a close approximation to the Carreau-Yasuda model within the intermediate shear rate regime is utilized instead. The parameters needed in order to execute the simulation under power law model are shown below:

- a) Consistency coefficient, k and power law index, n
- b) Reynolds number, Re
- c) Bulk Velocity, U_b (m/s)
- d) Density of fluid, ρ (kg/m^3)
- e) Specific heat, c_p (J/kg.K)
- f) Thermal conductivity, k ($\text{W/m}^\circ\text{C}$)

4.2.3 ESTIMATION OF VALUES

a) k and n values

Figure 7 is a rheogram showing the shear viscosity, μ (in units of Pa.s) versus shear rate, $\dot{\gamma}$ (in units of s^{-1}) for 0.3% PAA given by Keegan (2009) obtained via steady shear viscosity measurements using the TA Instruments Rheolyst AR-1000N, a rotational controlled-stress rheometer. A power law model is fit to these data within the intermediate shear-rate regime to obtain the approximate power law constants to be used in the numerical simulations. The power-law equation below represents an apparent or effective viscosity as a function of the shear rate (SI unit Pa.s).

$$\mu_{eff} = k\dot{\gamma}^{n-1} \dots\dots\dots (4)$$

μ_{eff} = effective viscosity (Pa.s)

k = flow consistency index (Pa.sn)

$\dot{\gamma}$ = shear rate (s^{-1})

n = flow behaviour index (dimensionless)

The model was fit to the rheological data essentially by minimizing the error between the experimental and model by arbitrarily varying the values of k and n . The error is calculated using equation 5 shown in the next page.

$$S_r = \sum \left(1 - \frac{n_{data}}{n_{model}} \right)^2 \dots\dots\dots (5)$$

The values for **k** and **n** are **0.718711Pa.sn** and **0.391529** respectively for 0.3% PAA. These values are only used for condition 1 (Tfluid = Twall).

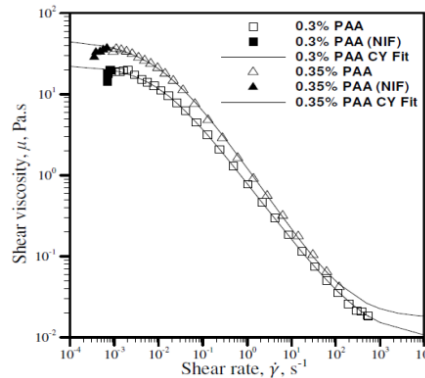


Figure 8: Shear viscosity versus shear rate graph for 0.3% polyacrylamide

For condition 2 (Tfluid ≠ Twall), the values of k and n are different as a different concentration of PAA is utilized due to availability of the temperature-viscosity data and correlation obtained from Mu-Hoe Yang (2000). Table below shows the values of n and k for 50ppm (0.005% w/w) PAA at respective temperature.

Temperature (°C)	K (Pa.sn)	n
20	0.00017696	1.45616
30	0.00021492	1.40388
40	0.00032959	1.34287
50	0.00066347	1.27945

Table 4: Values of k and n at different temperature

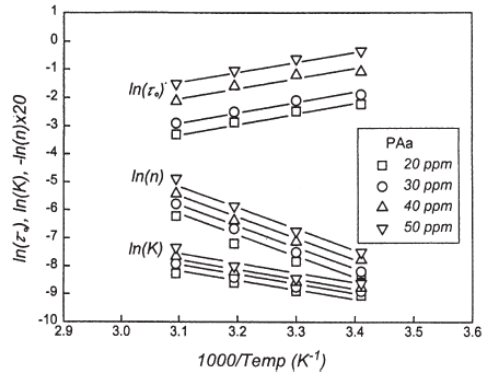


Figure 9: Temperature dependence of $\ln(t)$, $\ln(n)$ and $\ln(K)$ at different concentrations

b) Estimation of Reynolds Number

Reynolds number is defined as follows (Keegan (2009)):

$$Re = \frac{\rho U_b d}{\mu_{CH}} \dots\dots\dots (6)$$

Where: ρ is the fluid density (kg/m^3)

U_b is the bulk velocity at the end of the contraction (m/s)

d is the downstream duct height (mm)

μ_{CH} is characteristic shear viscosity (Pa.s)

Re	Flow Characteristics
$0 < 1$	Highly viscous, laminar ‘creeping flow
$1 < 100$	Laminar, strong Reynolds number dependence
$100 < 1000$	Laminar, boundary layer theory useful
$1000 < 10^4$	Transition to turbulence
$10^4 < 10^6$	Turbulent, moderate Reynolds number dependence
$10^6 < \infty$	Turbulent, slight Reynolds number dependence

Table 5: Flow characteristic for the respective range of Reynolds number (Keegan (2009))

For the simulation in Fluent, low Reynolds number is used to replicate laminar flow condition under creeping flow condition. The flow condition chosen for the investigation is **Re=5**.

c) The bulk velocity, U_b

The exact value for U_b is not indicated in the references. As for the time being, the bulk velocity is using trial and error values in order to obtain the cat's ear velocity profile. In this simulation, $U_b = 0.003\text{ms}^{-1}$ is used.

d) Density of fluid, ρ

Since the concentration of PAA solution is only 0.3% w/w, the solution is considered dilute. The later simulation for condition 2 ($T_{\text{fluid}} \neq T_{\text{wall}}$), lesser concentration of PAA (50 ppm) is used. Thus, the density of PAA solution is assumed to be the same as the density of water which is **999 kg/m³**.

e) Specific heat, c_p

Specific heat characterizes the amount of heat required to change a body's temperature by a given amount for example 1°C. The c_p values used in the simulation are the same as the c_p values of water at different temperature based on the assumption that the concentration of PAA is very low. Thus c_p values of PAA solution have very small variation compared to that of water. The table below shows the c_p values used in the simulation for condition 2.

Temperature (°C)	Cp (J/kg.K)
20	4183
30	4179
40	4179
50	4182

Table 6: Cp values at different temperature for 50 ppm PAA solution

f) Thermal conductivity, k

Thermal conductivity, k , is the property of a material that indicates its ability to conduct heat. The k value is assumed to be the same as water which is **0.58 W/m°C**.

4.2.4 RESULT

4.2.4.1 CONDITION 1

- $T_{\text{fluid}} = T_{\text{wall}}$
- 0.3% w/w PAA
- $U_b = 0.03\text{m/s}$
- Laminar flow
- $k = 0.718711\text{ Pa}\cdot\text{s}$
- $n = 0.391529$
- $c_p = 4183\text{ J/kg}\cdot\text{K}$

a) Trial 1

Simulation is run using the shorter version of contraction shown in Figure 6 and Figure 7. This design was used at the early stage of the project hereafter will be referred to as **Design 1 (D1)** The rectangular channels before and after the contraction are noticeably shorter than the latest version shown is Figure 5. The graph shown below is the velocity profile across span wise direction at several points along x-plane.

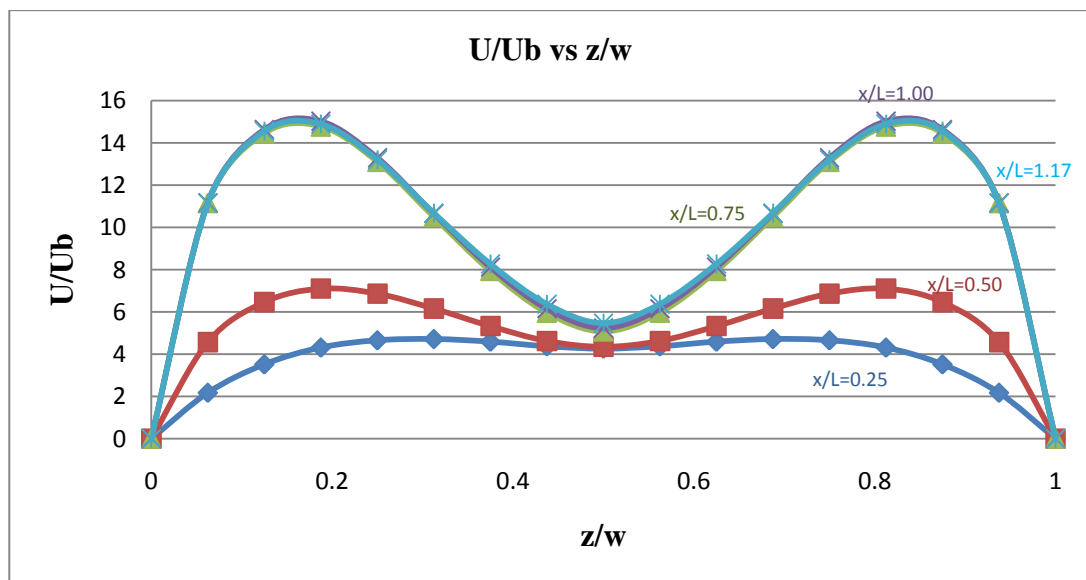


Figure 10: U/U_b versus z/w for D1 (condition 1)

Distance from the start of the gradual contraction, x .

x/L	0.25	0.50	0.75	1.00	1.17
$x(\text{mm})$	15	30	45	60	70

a) Trial 2

The latest contraction design is used in this simulation where both rectangular channels before and after the contraction are longer to ensure fully developed flow. The full length of contraction is shown in Figure 5 hereafter referred to as **Design 2 (D2)**. The graph shown below is the velocity profile across span wise direction at several points along x -plane.

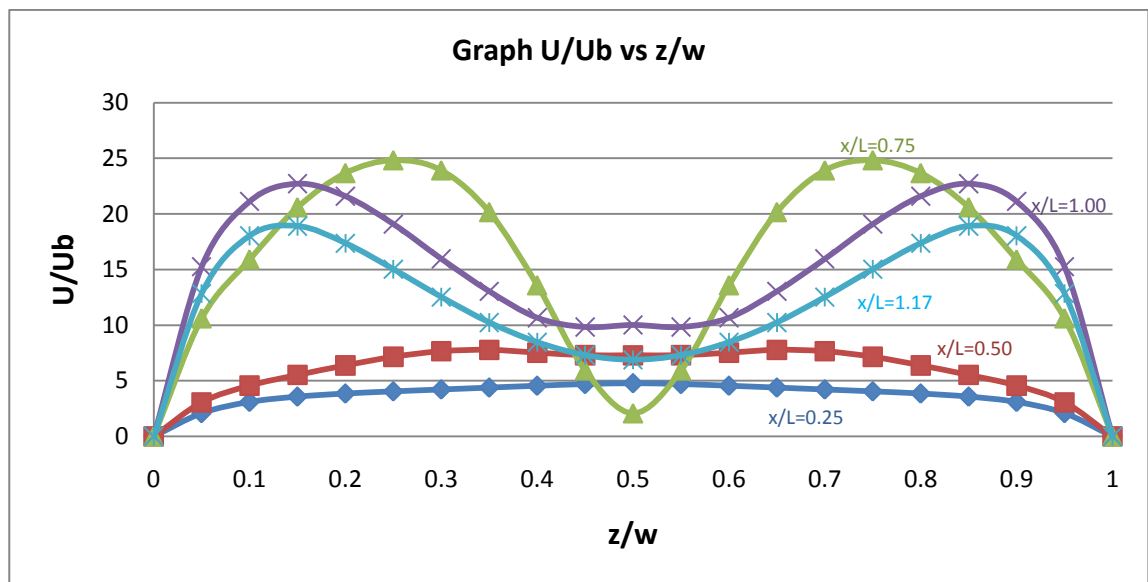


Figure 11: U/U_b versus z/w for D2 (condition 1)

Distance from the start of the gradual contraction, x .

x/L	0.25	0.50	0.75	1.00	1.17
$x(\text{mm})$	15	30	45	60	70

4.2.4.2 CONDITION 2

- $T_{fluid} \neq T_{wall}$
- k, n and c_p are shown in Table 4 and Table 6
- $n = 0.391529$
- $c_p = 4183 \text{ J/kg.K}$
- Geometry: D2
- 0.005% w/w (50ppm) PAA
- $U_b = 0.03 \text{ m/s}$
- Laminar flow
- Velocity profile is measured at 60mm from the start of contraction.

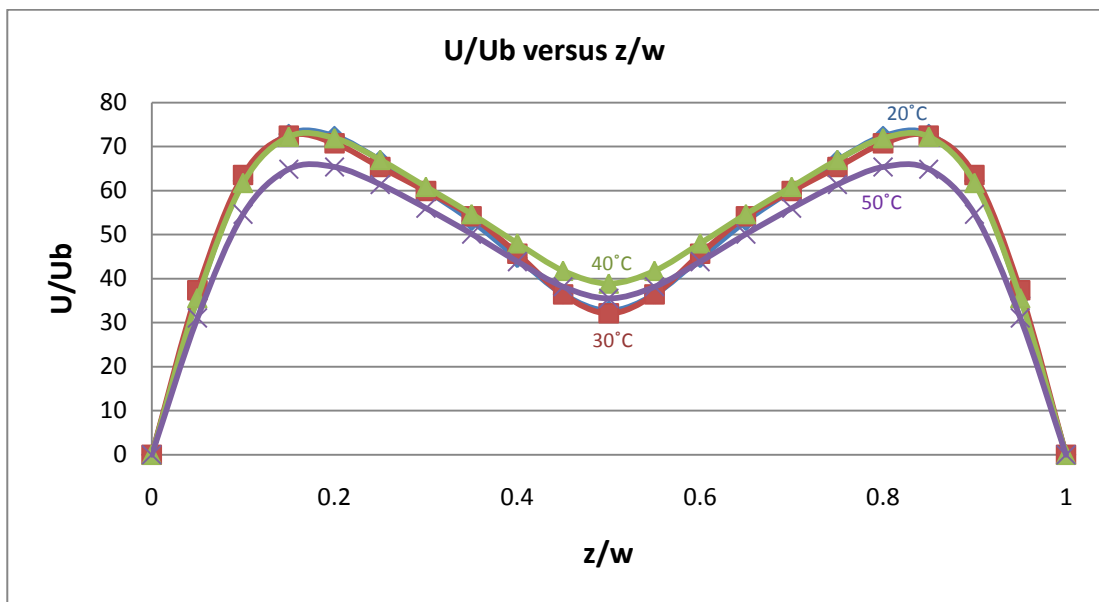


Figure 12: U/Ub versus z/w for condition 2

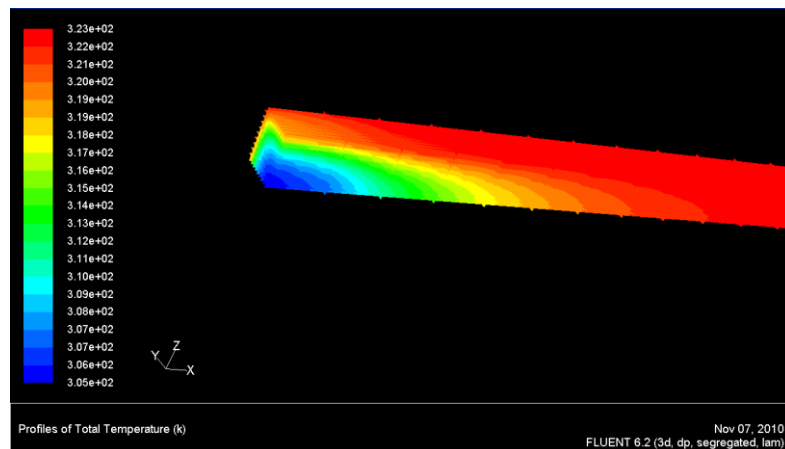


Figure 13: Temperature profile with $T_{wall}=50^{\circ}\text{C}$ and $T_{fluid}=27^{\circ}\text{C}$

4.3 DISCUSSION

4.3.1 CONDITION 1

D1 differs from D2 in terms of the length of rectangular channels before and after the contraction. A longer length before the contraction result in fully developed flow at the entrance of the contraction. Thus, D2 is selected for this advantage and is used in the subsequent simulations.

From both Figure 1 and 2, an extreme velocity overshoot near the contraction wall is observed at a distance from the beginning of contraction. For D1, clear velocity overshoot is observed at $x/L=0.5, 0.75, 1.00, \text{ and } 1.17$ which represent a distance of 30mm, 45mm, 60mm, and 70 mm from the start of contraction. For D1, clear velocity overshoot is observed at $x/L=0.75, 1.00, \text{ and } 1.17$ which represent a distance of 45mm, 60mm, and 70 mm from the start of contraction. The results indicate that the shorter the section before and after the contraction, the overshoot can be seen over a significantly longer length.

The results obtained above cannot be compared to the experimental results from Keegan (2009). Several parameters are differently defined such as the value of bulk velocity, U_b . This is due to unavailability of such information in the literature. However both simulations have proven that the cat's ear phenomenon can be replicated in Fluent given the right method and parameters.

4.3.2 CONDITION 2

In this simulation, 0.005% w/w (50ppm) PAA is used instead of 0.3% w/w PAA to conform to the literature by Mu-Hoe Yang (2000). The value of k and n for power law model are also taken from the same literature. These values vary according to the temperature and concentration.

The simulation is performed on four different wall temperatures; 20°C, 30°C, 40°C, and 50°C. Temperature distribution (Figure 13) confirms that the temperature of the fluid is gradually converging towards the temperature of the wall. At the starting of the contraction the value of the fluid is the same as the temperature of the wall.

The fluid velocity data for each wall temperature is taken at $x=60\text{mm}$ from the starting of the contraction. Figure 12 clearly shows the cat's ear phenomenon where extreme velocity overshoot is observed near the contraction wall. The graph also shows that as the temperature increases, the maximum value of the velocity overshoot decreases. The cat's ear phenomenon is more significant at a lower temperature. Moreover, the cat's ear phenomenon is observed for every temperature at the maximum distance which the velocity profile is measured i.e. 60mm.

CHAPTER 5

CONCLUSION AND RECOMMENDATION

As a conclusion, the cat's ear phenomenon is can be simulated in Fluent for a dilute concentration of polyacrylamide (PAA) solution. For both 0.3% w/w and 0.005% w/w PAA, velocity overshoot near the contraction wall is observed. As the temperature increases, the cat's ear effect is becoming less significant.

For further study on the subject, a better and accurate result can be obtained by doing mesh refinement study. It means that the mesh of the geometry is gradually refined until there is no variation on the simulation result. Moreover, a User Defined Function (UDF) can be developed to define the viscosity of the fluid based on the temperature-concentration correlations for power law model parameters i.e. k and n developed by Mu-Hoe Yang (2000).

Other than that, the Reynolds number should be calculated to match the flow condition defined by Keegan (2009) so that the simulation result can be compared with the literature. The calculation can be performed using equation 6 shown in section 4.2.3. The characteristic shear rate ($\dot{\gamma}_{CH}$) can be obtained from the simulation. The value of characteristic viscosity (μ_{CH}) corresponds to the characteristic shear rate. Please refer to page 59 of Keegan (2009) for more explanation.

REFERENCES

1. Meyers and Chawla, 1999, Mechanical behaviour of materials, pg.98-103.
2. Dusenbery and David B., 2009, Living at micro scale, Harvard University Press, Cambridge, Mass.
3. M. Reiner, 1964, The Deborah Number, Physics today vol.17, no.1, pg.62,
4. Reynolds, Osborne, 1883, An experimental investigation of the circumstances which determine whether the motion of water shall be direct or sinuous and of the law of resistance in parallel channels, Philosophical Transaction of the Royal Society, 174: 935–982.
5. S.A. Baeurle, A. Hotta, and A.A. Gusev, 2006, Polymer 47, 6243-6253.
6. R.J. Poole, M.P Escudier, 2004, Turbulent flow of viscoelastic fluid liquids through an asymmetric sudden expansion”, *J. Non-Newt. Fluid Mech.*117, 79.
7. R.J. Poole and Manuel A. Alves, 2009, Velocity overshoots in gradual contraction flows, *J. Non-Newt. Fluid Mech*, 160, 47-54.
8. Wisconsin Department of Transportation. Madison, 2001, Polyacrylamide as a Soil Stabilizer for Erosion Control, Report No. WI 06-98.
9. Walters, K., Bhatti, A.Q. and Mori, 1990, The influence of polymer conformation on the rheological properties of aqueous polymer solutions, Recent developments in structured continua, Vol. 2, Pitman, London.
10. Fiona Lee Keegan, 2009, Experimental investigation into non-Newtonian fluid through gradual contraction geometries, PhD Thesis, University of Liverpool, United Kingdom.

11. R.F. Legere, 1977, Reduction of water-oil ratio using polyacrylamides in vugular carbonate reservoirs, The Journal of Canadian Petroleum, PETSOC-78-04-04-P.
12. Mu-Hoe Yang, 2000, The rheological behavior of polyacrylamide solution II. Yield stress, Department of Chemical Engineering, Kao Yuan Institute of Technology, Kaohsiung County, 82101 Taiwan.
13. Dr Deryck Damian Patton, 2007, Acrylamide in fried, baked or roasted foods may increase risk of cancer in susceptible individuals, Internet Journal of Food Safety, Vol 9, p.14-16.